Arrangement of Filaments and Cross-links in the Bee Flight Muscle Z Disk by Image Analysis of Oblique Sections

James F. Deatherage,* Niaqian Cheng,‡ and Belinda Bullard§

*Department of Biochemistry, University of Arizona, Tucson, Arizona 85721; ‡Department of Biology, Peking University, Beijing, People's Republic of China; §European Molecular Biology Laboratory, 6900 Heidelberg, Federal Republic of Germany

Abstract. Information from oblique thin sections and from three-dimensional reconstructions of tilted, transverse thin sections (Cheng, N., and J. F. Deatherage. 1989. *J. Cell Biol.* 108:1761–1774) has been combined to determine the three-dimensional structure of the honeybee flight muscle Z disk at 70-Å resolution. The overall symmetry and structure of the Z disk and its relationship to the rest of the myofibril have been determined by tracing filaments and connecting elements on electron images of oblique sections which have been enhanced by a local crystallographic averaging technique. In the three-dimensional structure, the connecting density between actin filaments can be described as five compact, crystallographically nonequivalent domains. Features C1 and C2 are located on the transverse twofold rotation axes in the central plane of the Z disk. They are associated with the sides of actin filaments of opposite polarity. Features C3, C4, and C5 are present in two symmetry-related sets which are located on opposite sides of the central plane. C3 and C5 are each associated with two filaments of opposite polarity, interacting with the side of one filament and the end of the other filament. C3 and C5 may be involved in stabilizing actin filament ends inside the Z disk. The location of the threefold symmetric connection C4, relative to the thick filament of the adjacent sarcomere, is determined and its possible relationship to the C filament is considered.

THE Z disk of striated muscle cross-links and terminates thin filaments from adjacent sarcomeres. The Z disk of insect flight muscle, which is arranged on a hexagonal lattice, is structurally different from that of vertebrate muscle, which is arranged on a square lattice (Knappeis and Carlsen, 1962; Reedy, 1964). Although its hexagonal lattice is better ordered than the vertebrate muscle lattice, the insect flight muscle Z disk is a dense, low contrast specimen for electron microscopy.

There has been considerable uncertainty about the structure of the insect flight muscle Z disk. Its fine structure has been investigated in *Calliphora*, *Lethocerus*, and honeybee (Auber and Couteaux, 1963; Saide and Ullrick, 1973; Ashhurst, 1967*a*,*b*; reviewed by Ashhurst, 1977). The structures that have been proposed differ in many significant molecular details, including whether either (or both) thick and thin filaments (or extensions from their ends) participate in the Z disk network, and whether actin filaments enter and overlap inside the Z disk or terminate at its borders. Also unsettled are the nature of the cross-links (connecting filaments, tubes, or amorphous material) and the symmetries of the components of the network.

In this study we combine information from locally averaged oblique sections and three-dimensional reconstruction (Cheng and Deatherage, 1989) to construct a complete model for the honeybee Z disk.

Materials and Methods

Electron Microscopy and Image Processing of Oblique Sections

Thin sections of freshly dissected honeybee dorsal longitudinal indirect flight muscle were prepared for electron microscopy as described (Cheng and Deatherage, 1989). Electron microscopy and initial image processing were also carried out as described (Cheng and Deatherage, 1989). Background was flattened by high-pass filtering the image transforms. Regions of images with straight lattices across the Z disk and showing sharp diffraction maxima were selected for computer enhancement. If the lattice parameters varied across the image because of compression or distortion, the image was subdivided into well-ordered areas, the subdivisions were locally averaged, and the resulting locally averaged images were spliced together. Parallelograms of 5 × 5 adjacent unit cells were then locally averaged and the average displayed at the position of the central unit cell.

Local Averaging

Local running averages of the unit cells in a moving window were calculated and displayed together in a single modified image. This procedure has the precision of crystallographic averaging, but is continuous across the image. It is equivalent in effect to the photographic image-averaging method of Markham et al. (1964), in which photographic paper is shifted under the enlarger by multiples of the repeat of the motif to be enhanced, and repeatedly exposed. That is, the image is repeatedly shifted by multiples of a specimen unit cell and summed. Since sampling of the image by the microdensitometer generally does not correspond to an integral submultiple of the unit cell repeat, implementation of this type of averaging directly to the digitized image would require interpolation. However, the averaging can be im-

© The Rockefeller University Press, 0021-9525/89/05/1775/8 $2.00

plemented in the calculated Fourier transform of the image straightforwardly without interpolation, by applying a filter in Fourier space which is equivalent to convoluting with an exact window in image (real) space. The modified image in which the moving local averages are displayed can then be recovered by a second Fourier transformation.

The required real space averaging operation is as follows:

$$D'(x,y) = \sum_{M_1}^{M_2} \sum_{N_1}^{N_2} D(x + \Delta x, y + \Delta y)/N_w,$$

where $\Delta x = (M \cdot A_x + N \cdot B_x)$ and $\Delta y = (M \cdot A_y + N \cdot B_y)$. N_1 and N_2 are the beginning and ending unit cell steps defining the window along the specimen lattice A axis, counting in increments of one unit cell relative to the position in which the average density, D', will be displayed. M_1 and M_2 are the cell steps defining the window along the B axis. N_w is the number of unit cells in the window. A_x, A_y, B_x, and B_y are the components of the specimen lattice A and B axes along the x and y axes of the digitized image. D'(x,y) is the average of the density values at the corresponding fractional cell coordinates of all the unit cells in the window defined by M and N.

For a typical window M_1, $N_1 = -2$ and M_2, $N_2 = 2$, D'(x,y) is the average of the values of D(x,y) in the parallelogram of 25 unit cells centered on the unit cell containing D(x,y).

The equivalent averaging operation in the computed transform F(h,k) is as follows:

$$F'(h,k) = \sum_{M_1}^{M_2} \sum_{N_1}^{N_2} F(h,k) \exp(Q)/N_w,$$

where $Q = -2\pi i [h(x + \Delta x) + k(y + \Delta y)]$. The transform filtering term can be factored out as follows.

$$F'(h,k) = F(h,k) \sum_{M_1}^{M_2} \sum_{N_1}^{N_2} \exp(Q)/N_w.$$

The averaging operation is implemented by multiplying each structure factor of the image transform by the transform filtering term. For a symmetrical window, where $M_1 = -M_2$ and $N_1 = -N_2$, this term is real.

The moving average calculated by this procedure will be accurate throughout the image except where the window passes outside the image boundary. The calculated average specimen unit cell in the window will be accurate if the specimen and summation lattice repeats coincide, and if the lattice inside the window is coherent. This procedure has the advantage of producing averages over a precisely defined area. In pseudooptical filtering and similar simple transform-masking procedures, the average calculated reflects primarily the contents of unit cells in the immediate neighborhood, but also may contain out-of-phase or reverse-contrast contributions from all the unit cells in the image. This leads to uncertainty in interpretation because the exact features contributing to the moving average are poorly defined.

Results

The oblique sections we have examined enter the myofibril above the Z disk, pass through it, and exit below it. Three-dimensional information can be obtained by studying the change in projected density across the section, which corresponds to different levels of sectioning along the myofibril axis (Ashhurst, 1977; Saide and Ullrick, 1973). The oblique section in Fig. 1 samples the thin filament lattice from the A band into the Z disk. The oblique section in Fig. 2 samples the lattice through the Z disk. The thickness of these thin sections, estimated from their interference color, is ~500 Å. From the thickness of the Z disk, measured on longitudinal sections, and the diameter of the myofibril, we estimate the angle of cut to be between 2 and 3°. A density contour map of the micrograph in Fig. 2 after digitization and high-pass filtering is shown in Fig. 3.

Quite high resolution, three-dimensional information can be obtained from single oblique sections by the reconstruction method of Crowther and Luther (1984). However, this type of analysis requires perfectly aligned sections through an undistorted myofibril. Because the Z disk stains heavily and has relatively low contrast, selecting suitable oblique sections by visual inspection was impossible. We applied the local averaging technique, described in Materials and Methods, to our images to improve interpretability sufficiently to allow the local projected structure across the sections to be determined. Fig. 4 is a density contour map of the Z disk image shown in Figs. 2 and 3 after local averaging. Fig. 5 shows

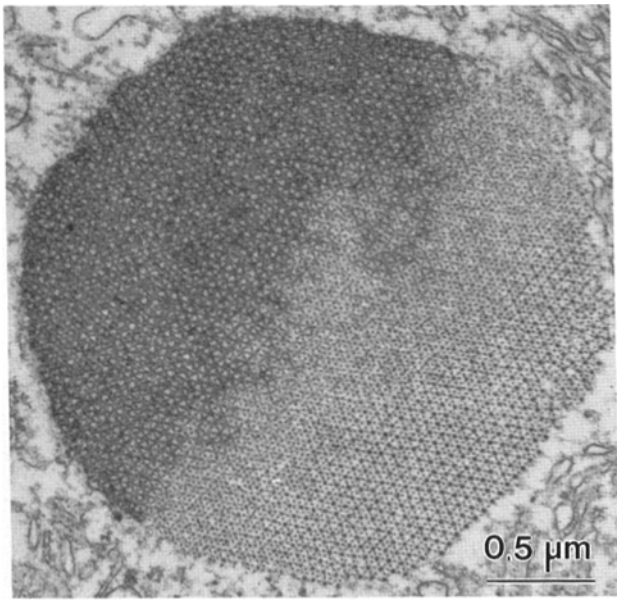

Figure 1. Oblique thin section of a honeybee flight muscle myofibril from the level of the Z band (upper left) to the A band (lower right).

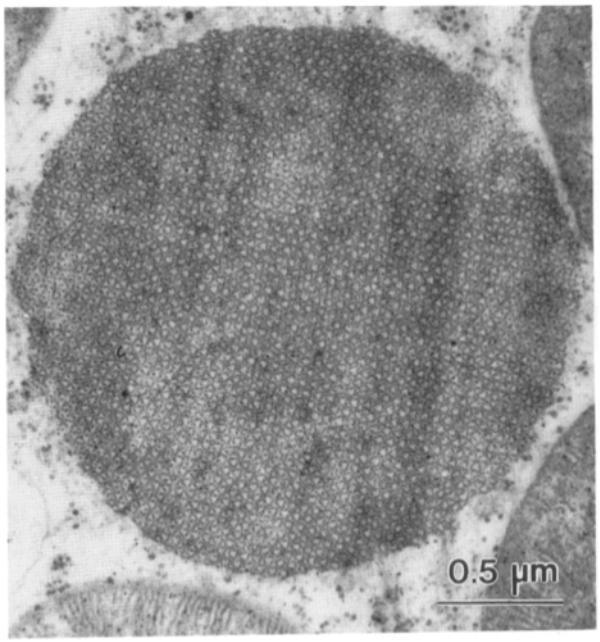

Figure 2. Oblique thin section through the Z band of honeybee flight muscle.

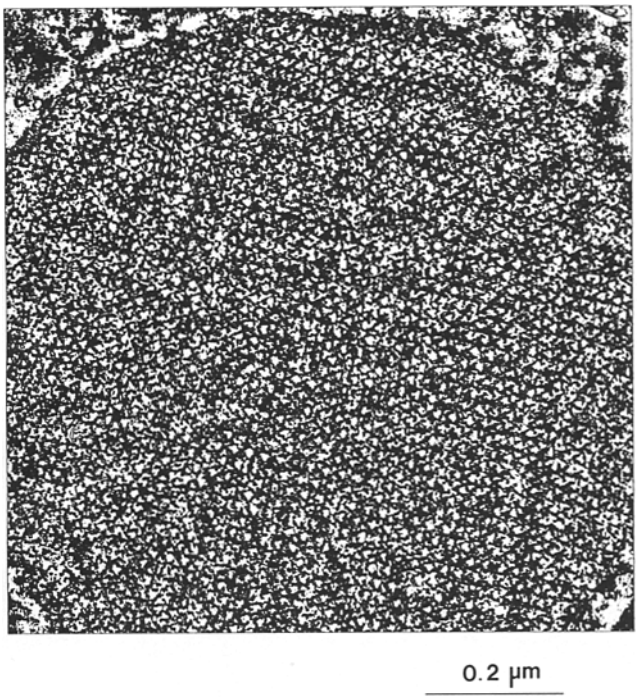

Figure 3. Contour map of the image in Fig. 2 after digitization and high-pass filtering.

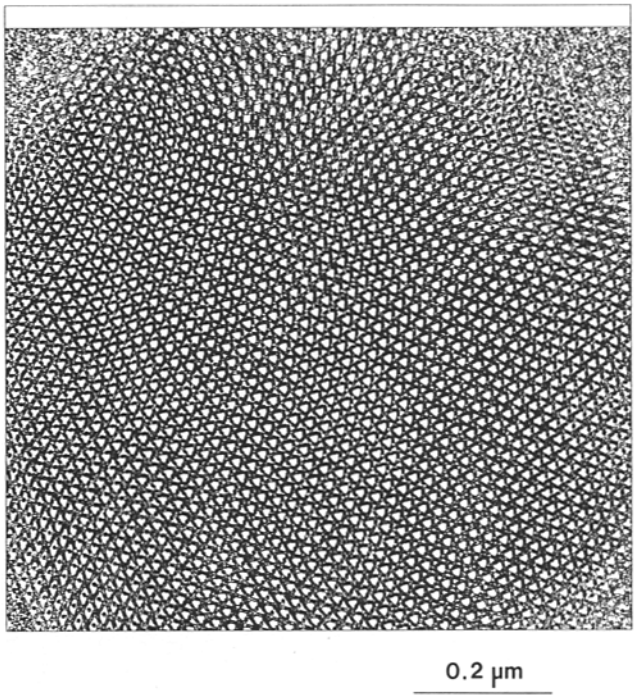

Figure 4. Contour map of the image in Figs. 2 and 3 after local averaging. Each unit cell contains the average of itself and the surrounding 24 unit cells. The contour levels are the same as in Fig. 2.

details from the left (Fig. 5 *a*), middle (Fig. 5 *b*), and right (Fig. 5 *c*) of the locally averaged map. Examination of the locally averaged maps showed that none of our oblique sections meet the criteria for analysis by Crowther and Luther's (1984) method. However, we found that the rough overall three-dimensional arrangement could be deduced from our locally averaged maps. This we combined with more detailed information from our three-dimensional reconstructions of the Z disk from images of tilted, thin sections (Cheng and Deatherage, 1989). The three-dimensional maps reconstructed from tilt series are quite detailed but cover only a limited axial range of the myofibril. They were extended using the symmetry and long range information available from the oblique sections to construct a complete model.

On images of oblique sections, the content of the unit cell varies across the myofibril. For sections which are close to transverse, the change is gradual, and neighboring unit cells in the lattice have nearly the same projected structure. To take advantage of this structural redundancy, parallelograms of 5 × 5 neighboring cells were locally averaged. The locally averaged images have a sufficiently improved signal-to-noise ratio to allow us to trace the arrangement of filaments and cross-links in three dimensions.

Filaments

Using images like those in Figs. 1 and 2, we traced the lattice of the myofibril continuously from the A band through the Z disk to the opposing A band. Our observations on the relative register of the thick and thin filament lattices of the A and Z bands are in agreement with those of previous investigators (Auber and Couteaux, 1963; Ashhurst, 1967*a*,*b*, 1977; Saide and Ullrick, 1973).

On the locally averaged images of oblique sections (Figs. 4 and 5) the lattice is hexagonal with a unit cell repeat of ~470 Å. There are three distinctly different patterns of projected density which succeed each other as the section traverses the Z disk (Fig. 5, *a*–*c*). Because they correspond to levels of the Z disk extending over an axial distance of ~800 Å, they are likely to reflect some molecular stratification of the network.

In the central region of the Z disk, the symmetry is 32 (Fig. 5 *b*); in the flanking regions the symmetry is 3 (Fig. 5, *a* and *c*). The actin filaments are the densest features in the images. From its A band of origin, the thin filament lattice can be traced through most of the Z disk to its end on the far side of the Z disk (Fig. 1). The lattices of the opposing sarcomeres which are joined at the Z disk have opposite orientations and are out of register by (1/3,1/3) unit cell. Across most of the Z disk, two sets of actin filaments are present in the lattice, consistent with overlap of filaments from opposing saracomeres inside the Z disk. Where both lattices overlap, the dominant motif is an approximately hexagonal bundle of six filaments of alternating polarity. These findings confirm similar previous observations of the filament lattice of *Lethocerus* and honeybee Z disks (Ashhurst, 1967*a*,*b*; Saide and Ullrick, 1973). The filament overlap which is inferred from oblique sections is confirmed by direct observation in the three-dimensional density maps reconstructed from images of tilted sections (Cheng and Deatherage, 1989).

Connections Between Filaments

Connections between filaments appear as lower density features in the maps (Figs. 5 and 6). These connections can be identified with the features observed on the three-dimensional reconstructions (Cheng and Deatherage, 1989) as

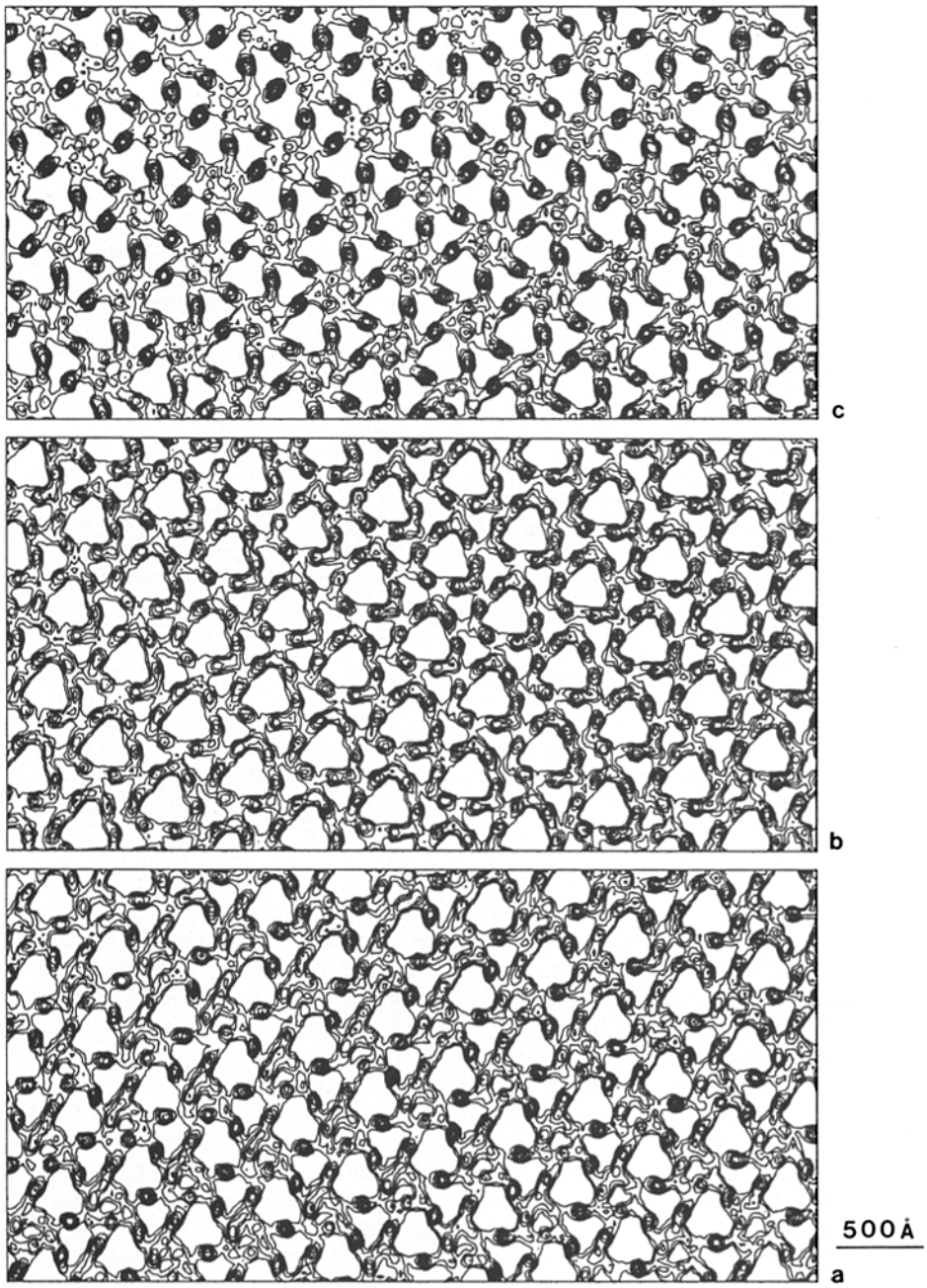

Figure 5. Magnified details from the left (*a*), middle (*b*), and right (*c*) of Fig. 4. *a* includes filaments from sarcomere B (the densest features), connections C3 and C5, and filaments from sarcomere A (lower density features than the filaments from sarcomere B). *b* includes filaments from both sarcomeres A and B and connections C1 and C2. *c* includes filaments from sarcomere A (the densest features), connections C3′ and C5′, and filaments from sarcomere B (lower density features than the filaments from sarcomere A).

connections C1, C2, C3, and C5 (Fig. 6). The threefold symmetric connection, C4, observed on the three-dimensional reconstructions does not show up on the oblique section maps. Because of its low density, averaging of >25 unit cells may be necessary to see this feature.

There are two connecting features lying on the twofold axes in the central plane of the Z disk (Figs. 5 *b* and 6 *b*). These correspond to features C1 and C2 in the three-dimensional density maps. C1 and C2 are each associated with a pair of neighboring filaments of opposite polarity. They alternate around the bundle of six filaments to form a triangular complex. C1 is displaced outwards towards the adjacent bundle of six filaments to form the apex of the triangle, and C2 inwards to form part of the base. At lower contour levels, density is continuous between connections C1 and C2 of adjacent bundles, suggesting they may be in contact.

Away from the center of the Z disk (Figs. 5 *a* and 6 *a*), another connection (corresponding to C3 in the three-dimensional density maps) connects a pair of filaments in adjacent bundles. On the other side (Figs. 5 *c* and 6 *c*), a symmetry-related cross-link (C3′) connects a different pair of filaments in the same bundles. The symmetry-related connections C5 and C5′ are also located in the flanking regions. All of C5, which is only partially included in the three-dimensional reconstructions, is seen in the oblique sections.

The densities for the groups of connections C3–C1–C3′ and C5–C2–C5′ appear to be continuous axially. There may be axial gaps in this density which are not observed. In this

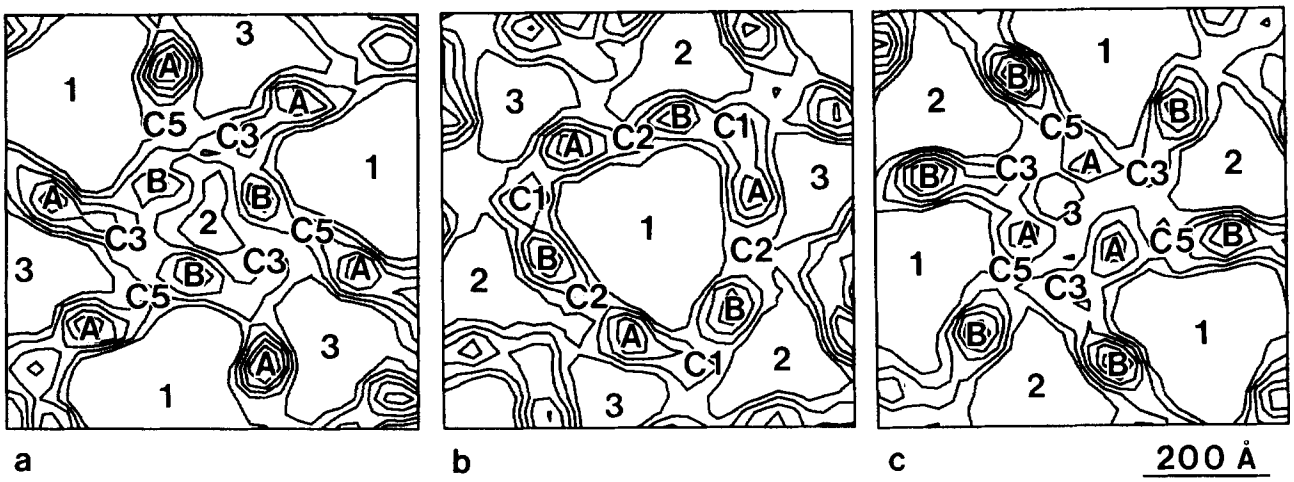

Figure 6. Magnified details of *a*, *b*, and *c* of Fig. 5. Filaments from sarcomeres A and B, and connecting density features C1, C2, C3, and C5 are labeled. *1*, *2*, and *3* mark special positions in the lattice that are aligned axially.

analysis of projections of oblique thin sections, axial structural details smaller than the thickness of the section may not be reliably detected.

Solvent Channels

The filaments and cross-links frame sets of large and small solvent channels in the Z disk. The largest channel is framed in the central plane of the Z disk by the approximately hexagonal bundle of six filaments of alternating polarity, and the alternating connections C1 and C2. Its overall shape is triangular. This channel passes entirely through the Z disk and is open at both ends. It is centered on the 32 position in the lattice and is bipolar.

The smaller channels pass most of the way through the Z disk, then taper down and pinch off. These channels are framed by three filaments of the same polarity grouped around a threefold axis. As it enters the Z disk, the interfilament spacing of this group of three filaments is 230 Å. Near the ends of the filaments on the far side of the Z disk, this spacing has decreased to 120 Å and the filaments are bundled into a tight triangular complex which pinches off the channel.

Discussion

Tracing lattices and symmetry elements on images of oblique sections like Figs. 1 and 2 defines the overall structure of the Z disk and its relationship to the adjacent A bands of the myofibril. We have identified corresponding features on the oblique sections and in the three-dimensional density maps obtained by reconstruction of tilted sections. Matching these features defines the axial position, symmetry, and register of the three-dimensional reconstructions in relation to the rest of the myofibril.

The honeybee Z disk is ~1,200 Å thick, and its central region of filament overlap is >800 Å thick. The major cross-linking protein of the Z disk, α-actinin, has a linker length of ~250–300 Å. α-Actinin can be fit in oblique orientations into the connecting density features in the three-dimensional reconstructions of tilted, transverse sections of the Z disk (Cheng and Deatherage, 1989). Even if α-actinin cross-links have a predominantly axial orientation in the structure, they would have to be organized into at least three layers to span the Z disk axially. There is evidence for stratification of connections from three-dimensional reconstructions of tilted, transverse sections into the layers (C3,C5), (C1,C2), and (C3′,C5′), but other axial packings are also possible (Cheng and Deatherage, 1989).

To simplify description of the three-dimensional reconstructions, the connecting density features have been defined as the compact domains C1–5, but this subdivision of the connecting density does not necessarily correspond to the molecular boundaries of the cross-links (Cheng and Deatherage, 1989). A schematic drawing of a unit cell of the three-dimensional structure is shown in Fig. 7. The filaments are shown with a reduced diameter to improve visibility. The centers of the connecting density features C1–5 are shown as circles with numbers. The axial extents of these features are not indicated in Fig. 7. The lines from the circles to the filaments indicate the strongest connectivity of the density features to the actin filaments. The simplest interpretation of the map is that features C1, C2, C3, and C5 each correspond to a predominantly axially oriented α-actinin molecule which is connected to the filaments indicated in Fig. 7 (Cheng and Deatherage, 1989). Other interpretations are also possible; an alternative interpretation of the connectivity of features C1 and C2 is shown in Fig. 8. These alternative interpretations cannot be distinguished at current resolution of our data.

Relationship of Connection C4 to the Thick Filament

Connections between the ends of the thick filaments and the Z line (C filaments) have been observed in thin sections of stretched rigor insect flight muscle (Reedy, 1971; White and Thorson, 1973). In longitudinal sections, these originate from the ends of the thick filaments and extend to the Z disk. In transverse sections, they are seen occupying positions in a lattice aligned with the thick filaments. Proteins in this region have also been detected immunologically (Bullard et al., 1977; Saide, 1981).

There are similar connections in vertebrate skeletal muscle as well (Locker and Leet, 1972). Titin and nebulin, high

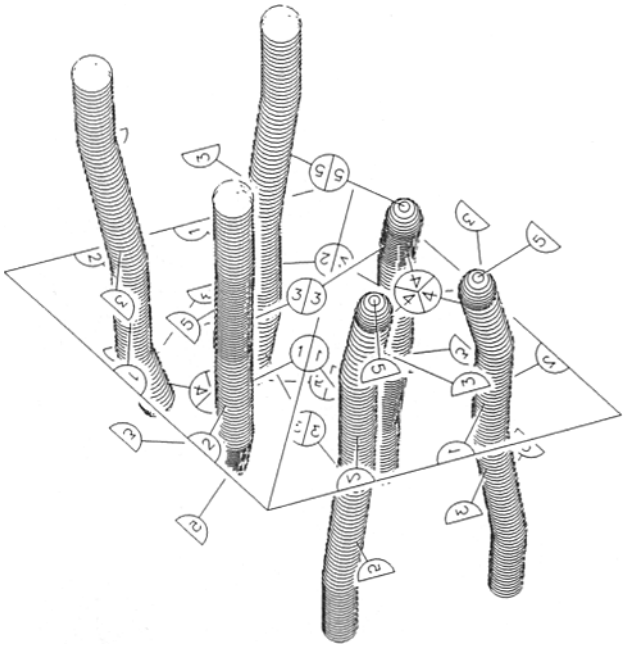

Figure 7. Model of a unit cell of filaments and connecting features of the Z disk. The actin filaments are shown with a reduced diameter to improve the visibility of the markers for the connecting density features. The connecting density features are indicated by circles and lines; the axial extent of the features is not shown. The lines from the circles to the filaments indicate the continuity of the connecting density on the three-dimensional maps. C1 and C2 lie on the twofold symmetry axes in the central plane of the Z disk; these rotation axes are indicated by lines. The symmetry-related pairs of asymmetric connecting features, C3 and C5, and threefold symmetric connections, C4, are indicated.

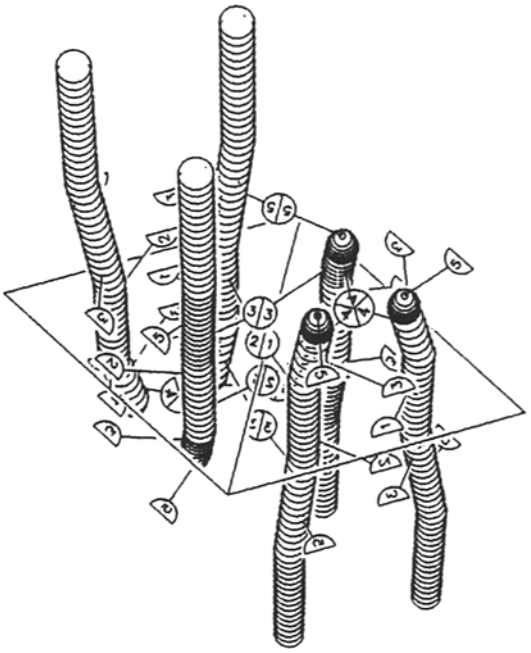

Figure 8. Similar model to Fig. 7, illustrating a different interpretation of the connectivity of features C1 and C2.

molecular weight components of vertebrate skeletal muscle myofibrils, have been suggested to form an elastic network within the myofibril (Wang, 1982). The end filaments described by Trinick (1981) are located at the end of the thick filament. They correspond in structure and location to titin, and are probably composed of titin (Trinick et al., 1984). Mauryama et al. (1985) have found that antibodies to a related preparation of titin (connectin) label thick filaments and their extensions out into the Z line.

From analysis of oblique sections like Fig. 1, it is known that C4 is centered on the same position in the Z disk lattice which a thick filament occupies in the adjacent A band lattice. Fig. 9 *a* illustrates the relationship of the Z and A band thick and thin filament lattices, including the relationship between a C filament extension of the thick filament and connection C4. In stretched rigor muscle, the C filament extensions from the ends of the thick filaments towards the Z disk are observed at this same position in the lattice (White and Thorson, 1973). The axial register of the thick filament is not precisely known. Its vertical position in the schematic drawings in Fig. 9 is arbitrary.

C4 is in the correct location to serve as the attachment site of the C filament, if the C filament extends this far into the Z disk lattice (Fig. 9 *a*; see Cheng and Deatherage, 1989). Other workers have observed structures at this location which they have interpreted as connecting filaments (Auber and Couteaux, 1963; Garamvölgyi, 1965), but these interpretations have been disputed (Ashhurst, 1971, 1977). We have not demonstrated the existence of such an attachment. The three-dimensional reconstructions do not extend far enough towards the A band to establish the existence of such a link (Cheng and Deatherage, 1989). C filaments are not seen in these oblique sections of unstretched, relaxed muscle. Different preparative procedures (different staining, use of stretched rigor muscle) and averaging of more unit cells may be necessary to observe them. It is possible that C filaments are anchored in some structural elements of the Z disk or I band which are closer to the A band than connections C3, C4, and C5, and that these elements are in turn attached to the Z disk. Further investigation of the structure of this region by three-dimensional reconstruction will be necessary to answer these questions.

The connecting complex C4 and its group of three filaments are involved in an extensive set of connections. Six arms radiate from the three filaments to the six surrounding filaments of opposite polarity. Three of these arms are cross-link C3. The other three arms are cross-link C5. Cross-link C4 is on the threefold axis between these filaments. As noted above, C4 is seen on the three-dimensional density maps but not on the oblique maps. The complex is illustrated in Fig. 9 *b*. If the thick filament is anchored at connection C4, then it, its six surrounding thin filaments, and three thin filaments from the opposing sarcomere are all linked together.

Previous Investigations of Z Disk Structure

The structure of the insect flight muscle Z disk has been the subject of nearly a dozen major investigations since 1963. As was noted in the introduction, there are fundamental disagreements about the most basic details of its structure. The organization of the Z disk of vertebrate striated muscle has been the subject of more than two dozen electron micro-

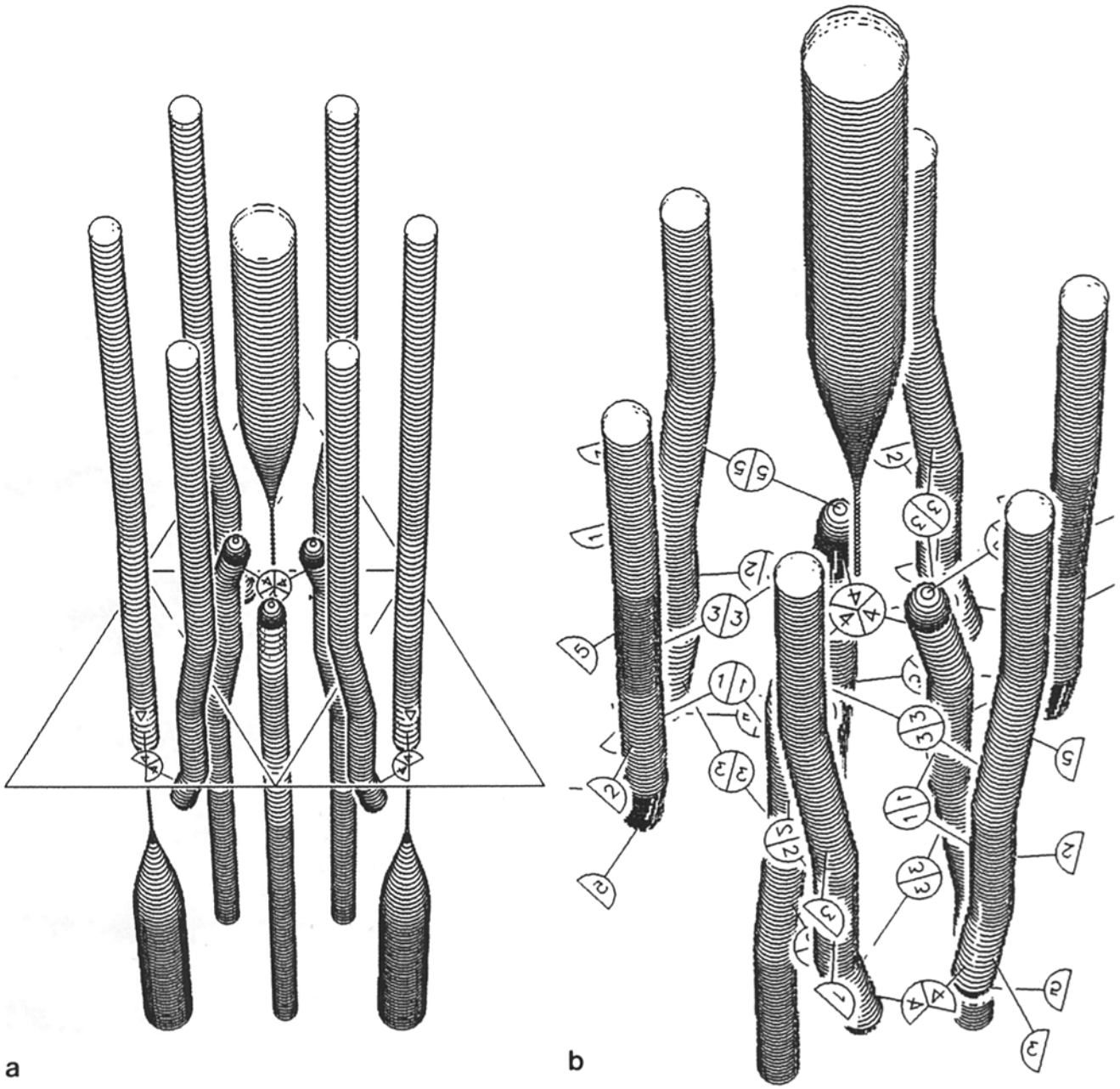

Figure 9. Diagrams indicating the relationships of the A and Z band lattices. The axial position of the thick filament is arbitrary. The C filament is shown as a slender extension from the end of the thick filament towards the Z disk. (*a*) Thick and thin filaments of the Z disk and both adjacent sarcomeres. (*b*) Details of the relationship of the Z disk connecting network to the thick filament and the C filament. A connection between the C filament and C4 has not been established.

scopic investigations since 1962. A number of fundamentally different molecular arrangements have been proposed for its structure as well.

The disagreements stem from a variety of causes. The major difficulty in these studies has been the interpretation of projection images at low resolution. Because the thickness of a section through a Z disk is densely packed with a complex arrangement of proteins, there is a large amount of superimposed structure in projection images. At low resolution, a variety of three-dimensional structures can be proposed which are consistent with projection images. However, unambiguous extrapolation from individual single-angle projection images to the unique correct three-dimensional structure, even for specimens much less complex than the Z disk, may be impossible. Visual inspection of such data can also lead to difficulties. In some cases features may be misidentified (see the review by Ashhurst, 1977).

There are other complicating factors. In insect flight muscle, the structure of the Z disk may differ between different species. The thin-sectioned Z disks in these species are similar in their basic pattern, but also show significant differences. In vertebrate muscle, there are structural differences between the Z disks of different muscle types. There is also evidence for at least two different tension-dependent, confor-

mational states of the vertebrate Z disk, which have been proposed to be interconvertable (MacDonald and Engel, 1971; Goldstein et al., 1982; Yamaguchi et al., 1985).

Our results are in agreement with previously described models for the filament lattices of the flight muscle Z disks of *Lethocerus* (Ashhurst, 1967*a*,*b*) and honeybee (Saide and Ullrick, 1973). As might be expected from its higher resolution, this study differs from Saide and Ullrick (1973) in its interpretation of the cross-linking structures of the lattice. An examination of the literature and our own unpublished micrographs suggest that flight muscle Z disk structure may vary with species and the physiological state of the muscle.

The structure of the vertebrate Z disk differs from that of insect. It has a square rather than hexagonal lattice and a different arrangement of filaments and cross-linking proteins. Because the lattices are different, the relative positions of filaments of opposite polarity in vertebrate striated and insect flight muscle Z disks differ. There are also differences in the arrangement of cross-links. In the vertebrate Z disk, curved or kinked cross-links connect actin filaments, but there is disagreement about their connectivity. Thick and thin vertebrate Z bands appear to be related in structure and to share a common axially repeating motif. There is evidence for only one type of cross-link, which is repeated by symmetry within and between the layers of the Z disk. This is in contrast to the insect structure, in which the connecting features and their environments are quite different from each other. The underlying structural similarities in cross-link stereochemistry may become more evident as higher resolution information is obtained from both the insect and vertebrate structures.

Self-assembly of the Z Disk

The connecting complexes C1 and C2 are centered on the crystallographic twofold rotation axes in the central plane of the Z disk and may nucleate the assembly of the Z disk. C1 and C2 may contain α-actinin, the symmetry of which may be responsible for the overall bipolar structure. Assembly of the central bipolar C1–C2 layer of the Z disk may fix the spacings and azimuthal orientations of the filaments in the lattice and provide specific interactions to direct the addition of successive layers of cross-links (C4, C3, and C5). With the exception of connection C4 near the filament ends, the connections in the network are between filaments of opposite polarity. It is likely that organization of the Z disk filament lattice is initiated by cross-links between groups of filaments of opposite polarity. Possible initial complexes are the groups of four filaments cross-linked by connections C1, C2, C3, and C5, or the bundle of six filaments cross-linked by connections C1, C2, and C5. It seems probable that formation of the bundles of three filaments of the same polarity is simply a consequence of the annealing of other units to form the network.

Connections C3, C4, and C5 may be responsible for determining the thickness of the structure. They may produce further displacements of actin filaments from their lattice positions in the central plane of the Z disk, imposing constraints on addition of more cross-links. Connections C3 and C5 bind near the filament ends and may cap them against further growth or depolymerization.

We thank Ms. P. Jansma for technical assistance.

This work was supported by National Institutes of Health grant AM33141; an American Heart Association (Arizona Affiliate) Grant-in-Aid to J. F. Deatherage; and a grant from the Muscular Dystrophy Group of Great Britain to B. Bullard.

Received for publication 28 December 1988.

References

Ashhurst, D. E. 1967*a*. Z-line of the flight muscle of belostomid water bugs. *J. Mol. Biol.* 27:385–389.

Ashhurst, D. E. 1967*b*. Erratum: Z-line of the flight muscle of belostomid water bugs. *J. Mol. Biol.* 30:441.

Ashhurst, D. E. 1971. The Z-line in insect flight muscle. *J. Mol. Biol.* 55: 283-285.

Ashhurst, D. E. 1977. The Z line: its structure and evidence for the presence of connecting filaments. *In* Insect Flight Muscle. R. T. Tregear, editor. North-Holland Publishing Co., Amsterdam. 57–73.

Auber, J., and R. Couteaux. 1963. Ultrastructure de la strie Z dans des muscles de dipteres. *J. Microsc. (Paris).* 2:309–324.

Bullard, B., J. L. Bell, and B. M. Luke. 1977. Immunological investigation of the proteins associated with thick filaments of insect flight muscle. *In* Insect Flight Muscle. R. T. Tregear, editor. North-Holland Publishing Co., Amsterdam. 41–52.

Cheng, N., and J. F. Deatherage. 1989. Three-dimensional reconstruction of the Z disk of sectioned honeybee flight muscle. *J. Cell Biol.* 108:1761–1774.

Crowther, R. A., and P. K. Luther. 1984. Three-dimensional reconstruction from a single oblique section of fish muscle M-band. *Nature (Lond.).* 307: 566–568.

Garamvölgyi, N. 1965. The arrangement of myofilaments in the insect flight muscle. *J. Ultrastruct. Res.* 13:409–424.

Goldstein, M. A., J. P. Schroeter, and R. L. Sass. 1982. The Z-band lattice of a slow skeletal muscle. *J. Muscle Res. Cell Motil.* 3:333–348.

Knappeis, G. G., and F. Carlsen. 1962. The ultrastructure of the Z disk in skeletal muscle. *J. Cell. Biol.* 13:323–335.

Locker, R. H., and N. G. Leet. 1972. Histology of highly-stretched beef muscle. *J. Ultrastruct. Res.* 52:64–75.

MacDonald, R. D., and A. G. Engel. 1971. Observations on organization of Z-disk components and on rod-bodies of Z-disk origin. *J. Cell Biol.* 48: 431–436.

Markham, R., J. H. Hitchborn, G. J. Hills, and S. Frey. 1964. The anatomy of tobacco mosaic virus. *Virology.* 22:342–359.

Mauryama, K., T. Yoshioka, H. Higuchi, K. Ohashi, S. Kimura, and R. Natori. 1985. Connectin filaments link thick filaments and Z lines in frog. *J. Cell Biol.* 101:2167–2172.

Reedy, M. K. 1964. Electron microscopic examination of the structure of the Z-band. *Proc. R. Soc. Lond. B Biol. Sci.* 160:458–460.

Reedy, M. K. 1971. Electron microscope observations concerning the behavior of the cross-bridge in striated muscle. *In* Contractility of Muscle Cells and Related Processes. R. J. Podolsky, editor. Prentice-Hall, Inc., Engelwood Cliffs, NJ. 229–246.

Saide, J. 1981. Identification of a connecting filament protein in insect fibrillar flight muscle. *J. Mol. Biol.* 153:661–679.

Saide, J. D., and W. C. Ullrick. 1973. Fine structure of the honeybee Z disk. *J. Mol. Biol.* 79:329–337.

Trinick, J. 1981. End-filaments: a new structural element of vertebrate skeletal muscle thick filaments. *J. Mol. Biol.* 151:309–314.

Trinick, J., P. Knight, and A. Whiting. 1984. Purification and properties of native titin. *J. Mol. Biol.* 180:331–356.

Wang, K. 1982. Myofilamentous and myofibrillar connections: role of titin, nebulin and intermediate filaments. *In* Muscle Development: Molecular and Cellular Control. M. L. Pearson and H. F. Epstein, editors. Cold Spring Harbor Laboratory, Cold Spring Harbor, NY. 439–452.

White, D. C. S., and J. Thorson. 1973. The kinetics of muscle contraction. *Prog. Biophys. Mol. Biol.* 27:173–255.

Yamaguchi, M., M. Izumimoto, R. M. Robson, and M. H. Stromer. 1985. The structure of wide and narrow vertebrate muscle Z-lines: a proposed model and computer simulation of Z-line architecture. *J. Mol. Biol.* 184:621–644.